



OPEN ACCESS

EDITED BY

Stuart C. Mangel,
The Ohio State University,
United States

REVIEWED BY

Archana Jalligampala,
University of Louisville, United States
Paul Werginz,
Vienna University of Technology,
Austria

*CORRESPONDENCE

David J. Calkins
david.j.calkins@vumc.org

SPECIALTY SECTION

This article was submitted to
Cellular Neurophysiology,
a section of the journal
Frontiers in Cellular Neuroscience

RECEIVED 10 June 2022

ACCEPTED 20 July 2022

PUBLISHED 05 August 2022

CITATION

Boal AM, McGrady NR, Risner ML and
Calkins DJ (2022) Sensitivity
to extracellular potassium underlies
type-intrinsic differences in retinal
ganglion cell excitability.
Front. Cell. Neurosci. 16:966425.
doi: 10.3389/fncel.2022.966425

COPYRIGHT

© 2022 Boal, McGrady, Risner and
Calkins. This is an open-access article
distributed under the terms of the
[Creative Commons Attribution License
\(CC BY\)](https://creativecommons.org/licenses/by/4.0/). The use, distribution or
reproduction in other forums is
permitted, provided the original
author(s) and the copyright owner(s)
are credited and that the original
publication in this journal is cited, in
accordance with accepted academic
practice. No use, distribution or
reproduction is permitted which does
not comply with these terms.

Sensitivity to extracellular potassium underlies type-intrinsic differences in retinal ganglion cell excitability

Andrew M. Boal, Nolan R. McGrady, Michael L. Risner and
David J. Calkins*

Department of Ophthalmology and Visual Sciences, Vanderbilt Eye Institute, Vanderbilt University Medical Center, Nashville, TN, United States

Neuronal type-specific physiologic heterogeneity can be driven by both extrinsic and intrinsic mechanisms. In retinal ganglion cells (RGCs), which carry visual information from the retina to central targets, evidence suggests intrinsic properties shaping action potential (AP) generation significantly impact the responses of RGCs to visual stimuli. Here, we explored how differences in intrinsic excitability further distinguish two RGC types with distinct presynaptic circuits, alpha ON-sustained (α ON-S) cells and alpha OFF-sustained (α OFF-S) cells. We found that α OFF-S RGCs are more excitable to modest depolarizing currents than α ON-S RGCs but excitability plateaued earlier as depolarization increased (i.e., depolarization block). In addition to differences in depolarization block sensitivity, the two cell types also produced distinct AP shapes with increasing stimulation. α OFF-S AP width and variability increased with depolarization magnitude, which correlated with the onset of depolarization block, while α ON-S AP width and variability remained stable. We then tested if differences in depolarization block observed in α ON-S and α OFF-S RGCs were due to sensitivity to extracellular potassium. We found α OFF-S RGCs more sensitive to increased extracellular potassium concentration, which shifted α ON-S RGC excitability to that of α OFF-S cells under baseline potassium conditions. Finally, we investigated the influence of the axon initial segment (AIS) dimensions on RGC spiking. We found that the relationship between AIS length and evoked spike rate varied not only by cell type, but also by the strength of stimulation, suggesting AIS structure alone cannot fully explain the observed differences RGC excitability. Thus, sensitivity to extracellular potassium contributes to differences in intrinsic excitability, a key factor that shapes how RGCs encode visual information.

KEYWORDS

retinal ganglion cells, excitability, potassium, physiology, action potential, glaucoma, axon initial segment

Introduction

The central nervous system is composed of many neuronal classes and types defined by genetic, neurochemical, morphologic, and physiologic properties that determine function. This biologic complexity is apparent across neural tissues and exemplified in the retina, which is a projection of the diencephalon. Different retinal neuronal classes and types interact through synaptic and electrical signals, forming local receptive fields. Receptive field elements converge, diverge, and converge again to optimize the signal-to-noise ratio of graded potentials received by postsynaptic retinal ganglion cells (RGCs) (Cohen and Sterling, 1990; Copenhagen et al., 1990; Asari and Meister, 2012). RGCs integrate postsynaptic potentials, generate spike trains that encode sensory information, and relay action potentials with high fidelity to central targets (Uzzell and Chichilnisky, 2004; Pillow et al., 2005). The presence of a large diversity in RGC response properties underlies the ability to encode complex visual scenes (Baden et al., 2016).

Currently, RGC types are distinguished by both intrinsic and extrinsic properties, including genetic profile, transcriptomics, morphology, regular topographic spacing, and physiologic response to stimuli (Sanes and Masland, 2015; Shekhar and Sanes, 2021). Based on these variables, 20–40 different RGC types of have been identified, depending on species (Sanes and Masland, 2015; Baden et al., 2016; Bae et al., 2018; Tran et al., 2019; Goetz et al., 2022). Measuring RGC response bias to light increments and decrements has been a mainstay in RGC taxonomy, but this method tests both extrinsic influences, such as presynaptic inputs, and intrinsic mechanisms, such as threshold for action potential generation. Alternatively, evidence suggests RGC types may be physiologically defined by measuring their responses to application of hyperpolarizing or depolarizing currents (Margolis and Detwiler, 2007; Mitra and Miller, 2007b,a; Cai et al., 2011). Testing these intrinsic properties is important because inherent differences can significantly influence spiking output in RGCs, establishing different light responses in cells with similar synaptic inputs (Emanuel et al., 2017; Werginz et al., 2020; Wienbar and Schwartz, 2022).

Here, we tested physiologic differences between two RGC types with distinct synaptic inputs, alpha ON-sustained (α ON-S) cells, which generate sustained firing of action potentials to light increments, and alpha OFF-sustained (α OFF-S) cells, which are inhibited by light and produce sustained firing upon light decrement. We found that these two types also demonstrate different intrinsic responses to application of depolarizing currents and correspondingly distinct AP waveforms. We also demonstrated that sensitivity to extracellular K^+ concentrations may mechanistically underlie these differences in excitability profiles and establish

thresholds for depolarization block, which is a mechanism that limits neuronal firing rate during excess depolarization due to inactivation of voltage-gated sodium channels. These results support the growing body of evidence that RGC responses are not only determined by presynaptic circuitry but also are significantly impacted by variability in intrinsic neuronal mechanisms.

Materials and methods

Animals

We obtained C57Bl/6J mice (6 male and 2 female, 14–17 weeks old) from Jackson Laboratories (Bar Harbor, ME, United States, RRID:IMSR_JAX:000664). Mice were housed at the Vanderbilt University Division of Animal Care and maintained on 12-h light/dark cycle. Animals were allowed water and standard rodent chow *ad libitum*. All animal experiments were approved by the Vanderbilt University Medical Center Institutional Animal Care and Use Committee.

Electrophysiological recordings

Animals were euthanized via cervical dislocation, eyes were enucleated, and the retinas were dissected out under long-wavelength illumination (630 nm, 800 μ W/cm², FND/FG, Ushio, Cypress, CA, United States). Retinas were placed in carbogen-saturated Ames' medium (US Biologic, Memphis, TN, United States) supplemented with 20 mM D-glucose and 22.6 mM NaHCO₃ (pH 7.4, 290 Osm). Each retina was mounted flat onto a physiological chamber, inner retina facing upward, and perfused at a rate of 2 ml/min with Ames' medium maintained at 35°C (Model TC-344C, Warner Instruments, Hamden, CT, United States).

Retinal ganglion cells were viewed under differential interference contrast (DIC) using an Andor charge-coupled device (CCD) camera attached to an Olympus BX50 upright microscope at 40 \times . RGCs were targeted for intracellular recording with pipettes pulled from borosilicate glass (I.D. 0.86 mm, O.D. 1.5 mm; Sutter Instruments, Novato, CA, United States) and filled with (in mM): 125 K-gluconate, 10 KCl, 10 HEPES, 10 EGTA, 4 Mg-ATP, 1 Na-GTP, and 0.1 ALEXA 555 (Invitrogen, Carlsbad, CA, United States). The intracellular solution pH was 7.35 and osmolarity was 285 Osm. Pipettes containing intracellular solution had a resistance between 4 and 8 M Ω . Whole-cell signals were amplified (Multiclamp 700B, Molecular Devices, San Jose, CA, United States) and digitized at a sampling rate of 10 kHz (Digidata 1550A, Molecular Devices, San Jose, CA, United States). Access resistance was monitored and maintained \leq 30 M Ω . All recordings were performed in current-clamp whole-cell patch-clamp configurations.

During baseline recordings we measured resting membrane potential (RMP), spontaneous spiking, light-evoked spike activity (full-field 365 + 460 nm, 300 $\mu\text{W}/\text{cm}^2$, 3-s duration, CoolLED, pE-4000, Andover, United Kingdom), and current-evoked spiking while clamping the cell at 0 pA. Current-evoked spiking was measured during stepwise application of 1 s current pulses, ranging from 0 to 300 pA in 10 pA increments, with a 2 s inter-stimulus interval. Very few $\alpha\text{OFF-S}$ cells exhibited sustained spiking at stimuli greater than 300 pA so we set that as the upper limit for recordings. Current was clamped at 0 pA between test pulses.

High extracellular potassium recordings

A second batch of Ames' medium was prepared as described above, but with an additional 5 mM of KCl (i.e., high K^+). After baseline recordings were completed for each cell, the high K^+ medium was washed into the recording chamber while the RGC spontaneous membrane voltage was continuously recorded. Before performing experiments, we allowed a wash on period of 5–6 min, allowing RGC membrane potential to stabilize. High K^+ experimental recordings (RMP, spontaneous activity, light-evoked spiking, and current-evoked spiking) were then performed as described above. After high K^+ experiments, the extracellular medium was switched back to the baseline solution, and RGC membrane voltage was continuously measured during a wash off period of 10–20 min, allowing RGCs to recover. Full recovery typically took 10–15 min, although it occasionally required up to 20 min. We limited the number of experimental protocols to reduce the time of high K^+ exposure. Furthermore, to limit potential cumulative effects of high K^+ wash on/off, we limited the total number of cells that were recorded from each retina to no more than four.

Retinal ganglion cell physiology analysis

Raw electrophysiology data files were analyzed in Python 3.9 (RRID:SCR_008394) using the pyABF 2.3.5 module (Harden, 2022) and SciPy 1.7.1 modules (RRID:SCR_008058) (Virtanen et al., 2020). The SciPy.Signal “find_peaks” function was used for AP detection with specified parameters of 20 mV minimum prominence and a distance threshold of 1.5 ms between spikes. Spike rates for current-evoked spiking protocols were reported as the average rate for 2 adjacent 10 pA increments of stimulation (20 pA bins). For AP shape analysis, a cubic spline function was fit to each AP waveform to increase resolution. The AP half-width was measured as the duration of the AP, in ms, where the membrane potential was above the midway point between each AP peak and minimum after-hyperpolarization.

Immunohistochemistry and imaging

After physiology, retinas were placed in 4% paraformaldehyde at 4°C for 24 h. After fixation, retinas were immunolabeled for choline acetyltransferase (ChAT, 1:100; Millipore, Burlington, MA, United States, Cat. #AB144P, RRID:AB_2079751) and ankyrin-G (AnkG, 1:200; NeuroMab N106/36; Antibodies, Inc. Cat. # 75–146, RRID:AB_10673030). Retinas were first blocked in 5% normal donkey serum for 2 h, then incubated in primary antibodies for 3 d at 4°C, and finally incubated for 2 h at room temperature with donkey anti-goat Alexa 647 and donkey anti-mouse Alexa 488 secondary antibodies (Jackson ImmunoResearch, West Grove, PA, United States; RRID:AB_2340437, RRID:AB_2341099). We used an Olympus FV1000 inverted microscope to obtain micrographs of RGC profiles. Image analysis, including creating orthogonal projections used for visualization of dendritic stratification depth, was performed using ImageJ (NIH, Bethesda, MD, United States). Soma size was determined in ImageJ by outlining the area encompassed by the soma in the maximum Z-stack projection from the confocal image of each dye-filled cell.

Axon initial segment measurements

Eight $\alpha\text{ON-S}$ and six $\alpha\text{OFF-S}$ cells had identifiable axon initial segment (AIS) labeling. Fluorescence of AnkG was measured from the edge of the soma along the axon of each RGC in ImageJ. Background fluorescence was subtracted from AnkG intensity profiles using a rolling ball filter with a radius of 50. Smoothed AnkG profiles were generated using a Savitzky-Golay filter with a first order polynomial fit. AIS bounds were systematically defined as the extent where smoothed ankG values were greater than 50% of the difference between baseline and maximum intensity. One $\alpha\text{ON-S}$ AIS was excluded from analysis as its length was identified as a significant outlier by Grubbs' Test ($\alpha = 0.05$).

Data analysis and statistical tests

All data are reported as mean \pm standard error of the mean (SEM) unless otherwise indicated. All statistical tests were performed in GraphPad Prism 9 (Graphpad Software, San Diego, CA). All data sets were checked for normality. Where appropriate, parametric statistical tests (unpaired *t*-test, paired *t*-test, 2-way ANOVA, simple linear regression) were performed. Additional statistical analysis was done performed using mixed-effects analysis where indicated. We defined statistical significance as a *p*-value of 0.05 or less. Exact *p*-values are indicated in figure legends, alongside the specific statistical test used for each analysis.

Results

Intrinsic cell type-specific differences in spike rate and waveform

We targeted α -type RGCs from intact retinas for whole-cell current-clamp recording and dye filling by identifying large cell bodies. Following physiology, we recovered morphology of dye-filled cells by confocal microscopy. As before (Risner et al., 2018, 2020, 2021, 2022), we separated RGC types based on soma size, dendritic stratification within the inner plexiform layer (IPL), and light-evoked responses. Here, we focused our analysis on two well-characterized α RGCs: α ON-S ($n = 11$ cells from 6 mice) and α OFF-S RGCs ($n = 6$ cells from 5 mice) (Krieger et al., 2017).

α ON-S RGCs possessed large cell bodies ($307.7 \pm 22.9 \mu\text{m}^2$) with dendritic arbors projecting within the proximal plexus formed by starburst amacrine cell dendrites, which we identified by ChAT labeling (Famiglietti and Kolb, 1976; Galli-Resta et al., 2000; Figure 1A). α OFF-S RGCs also possessed large somas ($209.2 \pm 16.2 \mu\text{m}^2$) although smaller than α ON-S RGC bodies ($p = 0.0089$). α OFF-S RGC dendritic arbors extended just beyond the distal ChAT band formed by starburst amacrine cell dendrites (Figure 1B). Similar to previous reports (Risner et al., 2020), we found α OFF-S RGC RMP significantly more depolarized vs. α ON-S RGCs (-55.2 ± 1.0 mV vs. -59.7 ± 0.8 mV, $p = 0.004$, Figure 1C). RMP variability was consistent with previously published results (Pang et al., 2003; Risner et al., 2018). In addition to RMP, α ON- and α OFF-S RGCs produced distinct voltage-gated responses to light stimulation. In the absence of light, α ON-S RGC produced few action potentials (2.56 ± 0.69 Hz), but these cells generated robust and sustained spiking during light onset (Figure 1D). α OFF-S RGCs spontaneously fired action potentials in the dark (12.61 ± 3.85 Hz), and light stimulation hyperpolarized membrane potential, reducing spiking. At light offset, α OFF-S RGCs membrane potential increased, and these cells produced a brisk sustained volley of spikes, returning to baseline firing after about 3 s (Figure 1E).

Similar to their light responses, RGCs also produce distinct responses to hyperpolarizing current injections (Mitra and Miller, 2007a; Margolis et al., 2010; Sladek and Nawy, 2020). Here, we investigated distinguishing properties of α ON- and α OFF-S RGCs in response to depolarizing currents (Twyford et al., 2014; Kameneva et al., 2016). We performed current-clamp (0 pA) recordings and measured responses of α RGCs to 1 s pulses of depolarizing current, ranging from 0 to 300 pA. We noticed α ON-S RGCs typically required strong depolarizing currents to induce robust spiking (Figure 2A, left). To the counter, α OFF-S RGCs often produced a sustained train of action potentials in response to relatively small depolarizing current injections, but larger depolarizing currents often reduced spiking (Figure 2A, right). In addition to

stimulus strength increasing variability in spike rate, we noted strong depolarizing currents increased variability in spike shape (Figure 2A, right). We quantified the relationship between test current and spike rate of α ON- and α OFF-S RGCs. We found a significant interaction between cell type and test current ($p < 0.0001$), indicative of cell type-intrinsic differences in excitability (Figure 2B). To control for the potential influence of differing RMPs on these results (see Figure 1C), we selected a subset of cells from each type with similar RMPs (-57 ± 1 mV, Figure 2C) for comparison. We found that the current-spiking relationships of this subset closely resembled the pattern of the full sample of cells (Figure 2D), and we did not detect a significant difference in current-evoked spike rates for the subset vs. full sample for either α ON-S ($p = 0.9317$) or α OFF-S RGCs ($p = 0.9618$).

As mentioned above, we noticed relatively small test currents appeared to impact α OFF-S RGC AP shape more than α ON-S RGC APs. We determined if depolarizing currents distinctly affect α ON-S vs α OFF-S RGCs by averaging AP waveforms at each test current. α ON-S RGC AP waveforms remained relatively similar across test currents (Figure 3A). During the duration of larger test currents, α ON-S RGC AP half-width modestly increased, though remained consistent (Figure 3B). The AP width of α OFF-S RGCs, however, grew larger with increasing depolarization (Figure 3C). Interestingly, at larger currents, α OFF-S AP half-width variability appeared greater compared to α ON-S RGCs (Figure 3D). To quantify this variability, we determined the coefficient of variation (CV) of AP half-widths for each stimulus. We found as depolarization increased, the variability of α OFF-S RGC AP half-width significantly increased compared to α ON-S RGCs ($p < 0.0001$, Figure 3E).

Others have found spike rate influences AP shape (de Polavieja et al., 2005). Because we found current-evoked spike rate is dependent on cell type (Figure 2), we measured the influence of spike rate on AP half-width for both α ON- and α OFF-S RGCs to determine if differences in AP width could be explained solely by firing rate (Figure 3F). We found α OFF-S RGC AP half-widths significantly increased as spike rate increased ($p < 0.0001$). To the counter, α ON-S RGC AP half-widths remained relatively stable as spike rate increased ($p = 0.0668$). These data suggest α ON- and α OFF-S RGCs can be distinguished, in regard to AP width, by their dependence on spike rate.

Sensitivity to K^+ determines retinal ganglion cell type-specific differences in spike rate and waveform

Rate-dependent spike widening is largely mediated by K^+ currents during action potential repolarization (Ma and Koester, 1996). Based on this premise, we determined if

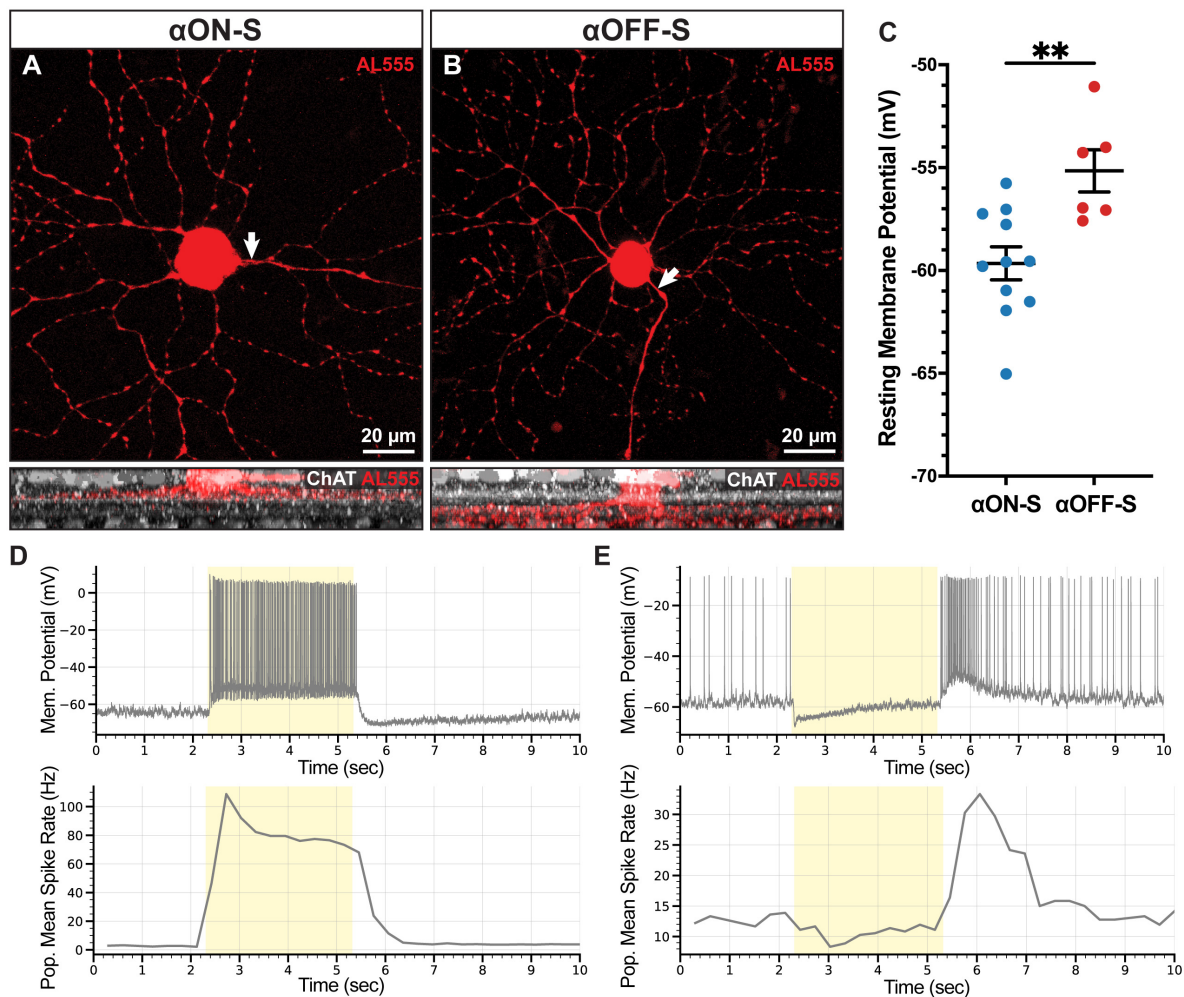


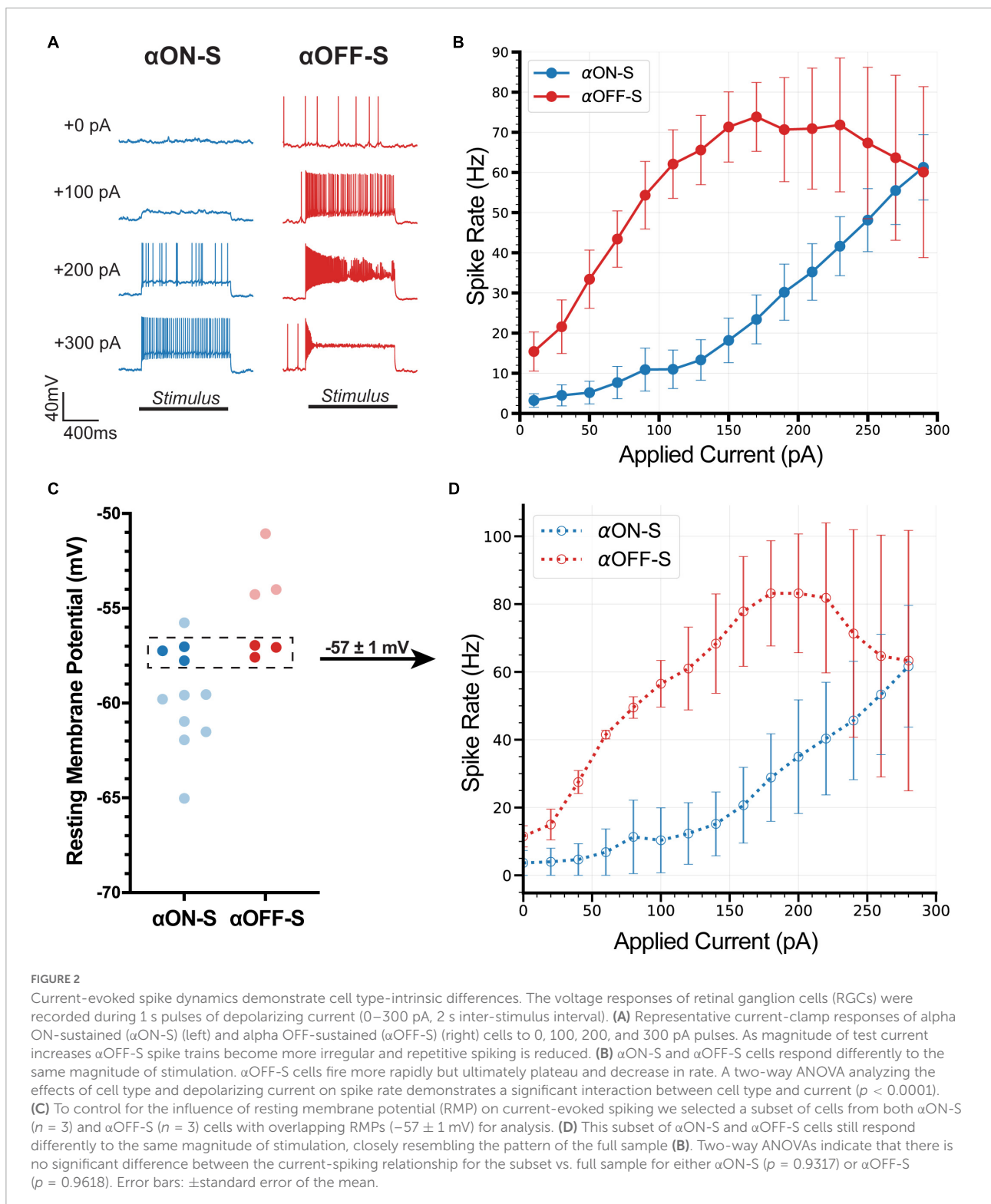
FIGURE 1

Morphologic and physiologic characterization of retinal ganglion cells (RGCs). Patched cells were filled with Alexa-fluor 555 dye (AL555, red) and morphologically reconstructed with confocal microscopy. (A,B) Representative maximum intensity projections of alpha ON-sustained (α ON-S) and alpha OFF-sustained (α OFF-S) RGCs demonstrate characteristic soma size and dendritic branching patterns (upper). White arrows indicate the axonal projection. Orthogonal projections of representative AL555-filled cells co-labeled for choline acetyltransferase (ChAT, white) demonstrate the branching of α ON-S and α OFF-S dendrites in the ON- and OFF-sublaminae of the inner plexiform layer, respectively (lower). (C) α OFF-S RGCs have a more depolarized resting membrane potential (mean = -55.2 mV, $n = 6$) than α ON-S (mean = -59.7 mV, $n = 11$) ($p = 0.004$, unpaired t -test). Error bars \pm standard error of the mean. (D,E) Representative current-clamp traces of the responses of α ON-S (D, upper) and α OFF-S (E, upper) RGCs to full-field light stimulation (yellow span) show the characteristic light responses of the two cell types. Mean firing rates of all α ON-S (D, lower) ($n = 11$) and α OFF-S (E, lower) ($n = 6$) binned into 200 ms intervals during light stimulation (yellow). $**p < 0.005$.

modulating the K^+ concentration gradient could explain cell type-specific differences in RMP, spike rate, and spike width. We employed a within-subjects approach where recordings were performed before and after bath application of extracellular medium containing additional KCl (extra 5 mM, high K^+ , Figure 4A). The additional 5 mM K^+ in this experimental approach brought the total extracellular K^+ concentration to 8 mM, making this treatment a physiologic depolarizing stimulus (Heinemann and Lux, 1977). High K^+ significantly depolarized RMP of both cell types ($p < 0.0001$ for both, Figure 4B). Notably, RMP of α ON-S and α OFF-S cells did not appear equally affected by high K^+ treatment. We analyzed

this apparent difference by computing the difference in baseline and high K^+ RMP (Δ RMP). We found Δ RMP of α OFF-S cells significantly greater than α ON-S RGCs ($p = 0.0038$, Figure 4C).

We next sought to determine how differences in sensitivity to high K^+ on RMP may influence current-evoked spiking of α RGC types. We measured spiking using the same depolarizing current stimulation protocol described earlier (Figure 2). High K^+ treatment not only increased spontaneous spiking of α ON-S RGCs, but also increased spiking at smaller test currents and appeared to cause depolarization block at test currents where it previously did not occur (Figure 5A). Overall, we



found high K^+ significantly altered the test current-spike rate relationship of α ON-S RGCs ($p = 0.0397$, **Figure 5B**). High K^+ treatment also dramatically altered α OFF-S cell current-induced spiking. Increasing test current strength in α OFF-S cells caused

depolarization block, reducing spike rate and increasing the number of failed APs (**Figure 5C**). Overall, we found high K^+ significantly changed the test current-spike rate relationship of α OFF-S RGCs ($p = 0.0005$, **Figure 5D**).

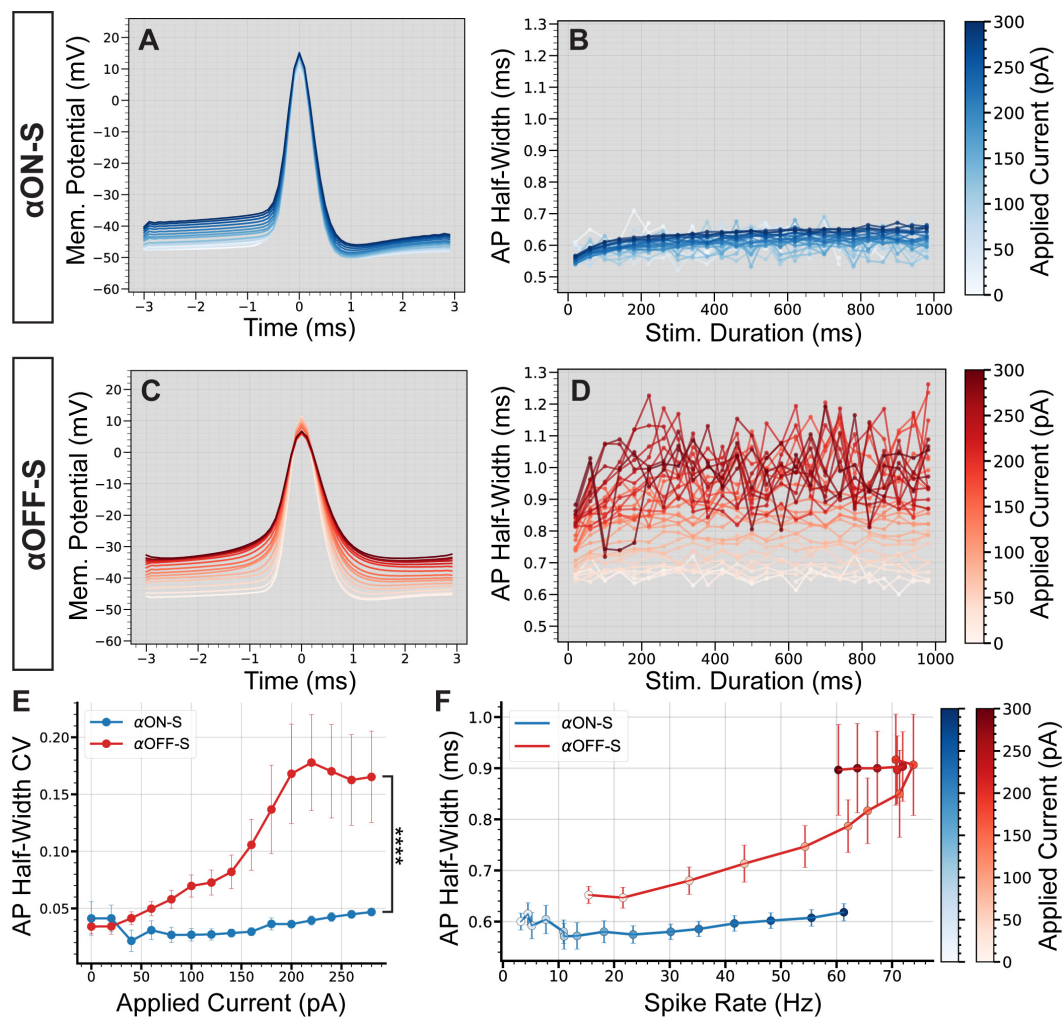


FIGURE 3

Cell type-specific differences in firing dynamics are reflected in the action potential shape. (A) Mean action potential (AP) shapes for alpha ON-sustained (αON-S) cells at each current step. (B) Mean AP half-width vs. stimulus duration for each current level of αON-S cells. (C) Mean AP shapes for alpha OFF-sustained (αOFF-S) cells at each current step. (D) Mean AP half-width vs. stimulus duration for each current level of αOFF-S cells. (E) AP half-width coefficient of variation (CV) vs. applied current for αON-S and αOFF-S cells. As depolarization increases, the variability of AP width increases significantly more for αOFF-S cells than αON-S (Mixed effects analysis interaction between current and cell type, $p < 0.0001$). (F) The mean spike rate at each current injection vs. the AP half-widths. αOFF-S retinal ganglion cells (RGCs) demonstrate significant rate-dependent spike widening (simple linear regression, non-zero slope $p < 0.0001$) while αON-S RGCs do not ($p = 0.0668$). Error bars = mean \pm standard error of the mean. **** $p < 0.0001$.

Finally, we investigated the impact of high K^+ on spike rate and AP shape. In addition to increasing spike rate and facilitating depolarization block (Figure 5), high K^+ augmented AP width in αON-S cells (Figure 6A). Similar to αOFF-S RGC APs produced under baseline conditions (Figure 3D), we observed high K^+ treatment not only increased αON-S cell AP half-width but also increased variability, especially at larger test currents (Figure 6B). High K^+ also increased αOFF-S cell AP width (Figure 6C) and considerably decreased αOFF-S spiking, essentially eliminating sustained spiking at stronger depolarizations (Figure 6D). Interestingly, under high K^+ conditions αON-S cells demonstrated a significantly linear

correlation between spike rate and AP width (Figure 6E)—similar to αOFF-S cells under baseline conditions (Figure 3F). Furthermore, the relationship between current and AP half-width CV of αOFF-S cells under baseline conditions and αON-S cells treated with high K^+ was not statistically different ($p = 0.719$, Figure 6F).

Evidence suggest intrinsic excitability of RGCs is in part due to AIS morphology (Werginz et al., 2020; Wienbar and Schwartz, 2022). In particular, the scaling of the AIS in α-sustained cells is important for fine tuning spiking thresholds and varies systematically by retinal topography (Raghuram et al., 2019). To evaluate the potential influence of AIS scaling on our

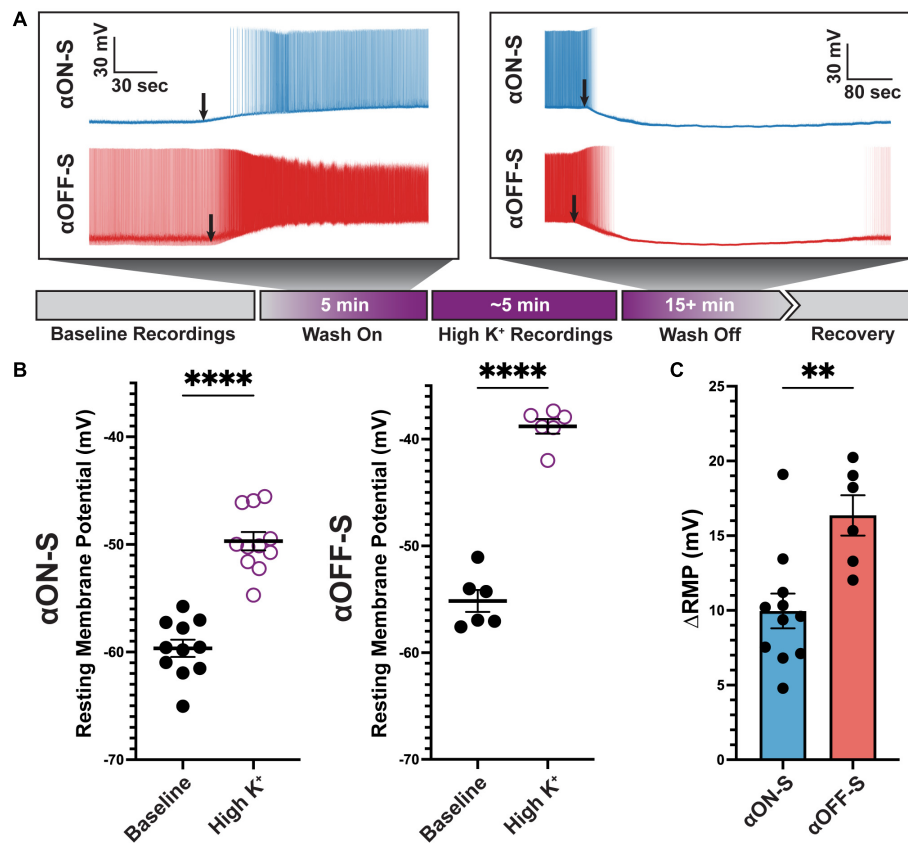


FIGURE 4

Alpha OFF-sustained (α OFF-S) cells are more depolarized by elevated extracellular potassium. (A) Schematic timeline of experiment, and representative spontaneous voltage responses of alpha ON-sustained (α ON-S) and α OFF-S cells during high K^+ medium (additional 5 mM KCl) wash on and off. Black arrows indicate onset of significant depolarization (left) or repolarization (right). (B) Resting membrane potentials (RMP) measured for each cell before and after addition of 5 mM KCl. High K^+ significantly depolarized both α ON-S and α OFF-S cells (paired t -tests, $p < 0.0001$ for both). (C) Change in RMP (Δ RMP) after high K^+ addition. Δ RMP was significantly greater for α OFF-S cells (unpaired t test, $p = 0.0038$). Error bars: \pm standard error of the mean. **** $p < 0.0001$, ** $p < 0.005$.

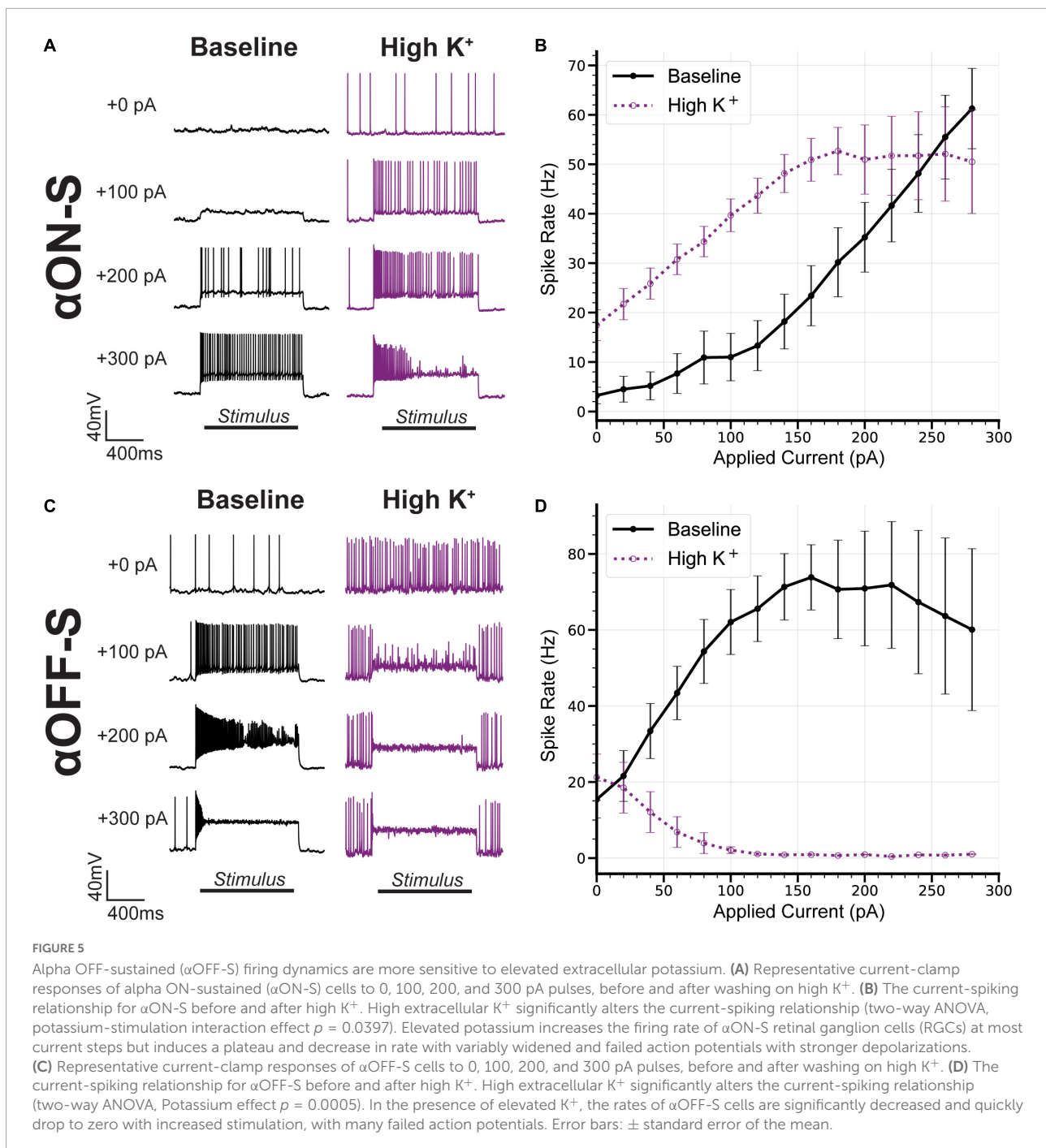
results we labeled recorded cells for AnkG, a scaffolding protein that defines the AIS (Figures 7A,B; $n = 7$ α ON-S, $n = 6$ α OFF-S). We measured AIS distance from soma and length based on AnkG immunofluorescence. We did not detect a significant difference between AIS distance from the soma (Figure 7C, $p = 0.3897$) or AIS length (Figure 7D, $p = 0.1145$) between α ON- and α OFF-S RGCs. Because the length of the AIS is linked to threshold for AP generation (Jamann et al., 2021) as well as a higher threshold for depolarization block (Werginz et al., 2020; Wienbar and Schwartz, 2022) we investigated the relationship between AIS length and current-evoked spiking in our cells. We used linear regression to determine the slope of this relationship at each test current (Figure 7E). At smaller test currents (0–140 pA) α OFF-S cells had a positive correlation between AIS length and spike rate, whereas there was a moderately negative correlation for α ON-S cells (Figure 7F). However, at larger test currents (180–300 pA) the relationship for α OFF-S cells flipped, with cells with longer AISs exhibiting lower spike rates. R^2 values for regressions (Figure 7G) were moderately high (0.35–0.61)

for α OFF-S except at test currents correlating with the onset of depolarization block (160–180 pA, $R^2 = 0.05$ –0.20), while they were fairly low at all currents for α ON-S cells (0.06–0.20).

Discussion

Alpha ON-sustained and alpha OFF-sustained retinal ganglion cells exhibit distinct excitability profiles and spike waveforms

Our findings indicate α ON-S and α OFF-S RGCs maintain distinct RMPs and voltage-gated responses to depolarizing currents, in addition to differences in light-evoked activity (Figures 1, 2). We found α OFF-S RGCs produced more robust responses to small depolarizing currents compared to α ON-S RGCs (Figure 2). This difference is driven by more than



simply the higher spontaneous activity of α OFF-S in these recording conditions since the slope of the increase in rate is greater for α OFF-S than α ON-S cells (Figure 2B). In response to larger current injections, α OFF-S RGCs often produced few full spikes, followed by aborted action potentials, and sustained membrane potential, indicating depolarization block. To the counter, α ON-S RGC responses remained robust to large current injections (Figure 2). These differences persisted even when controlling for RMP (Figures 2C,D) lending support to

RGC-intrinsic mechanisms driving differences in spike rate and depolarization block. While our interpretations are limited by our sample size, these findings confirm and extend the evidence that ON and OFF RGC responses are differentially dependent on stimulus amplitude (Twyford et al., 2014; Kameneva et al., 2016).

In addition to spike rate, we found α ON-S and α OFF-S RGC AP width to be differentially dependent on stimulus strength. α OFF-S RGC AP half-width dramatically increased as

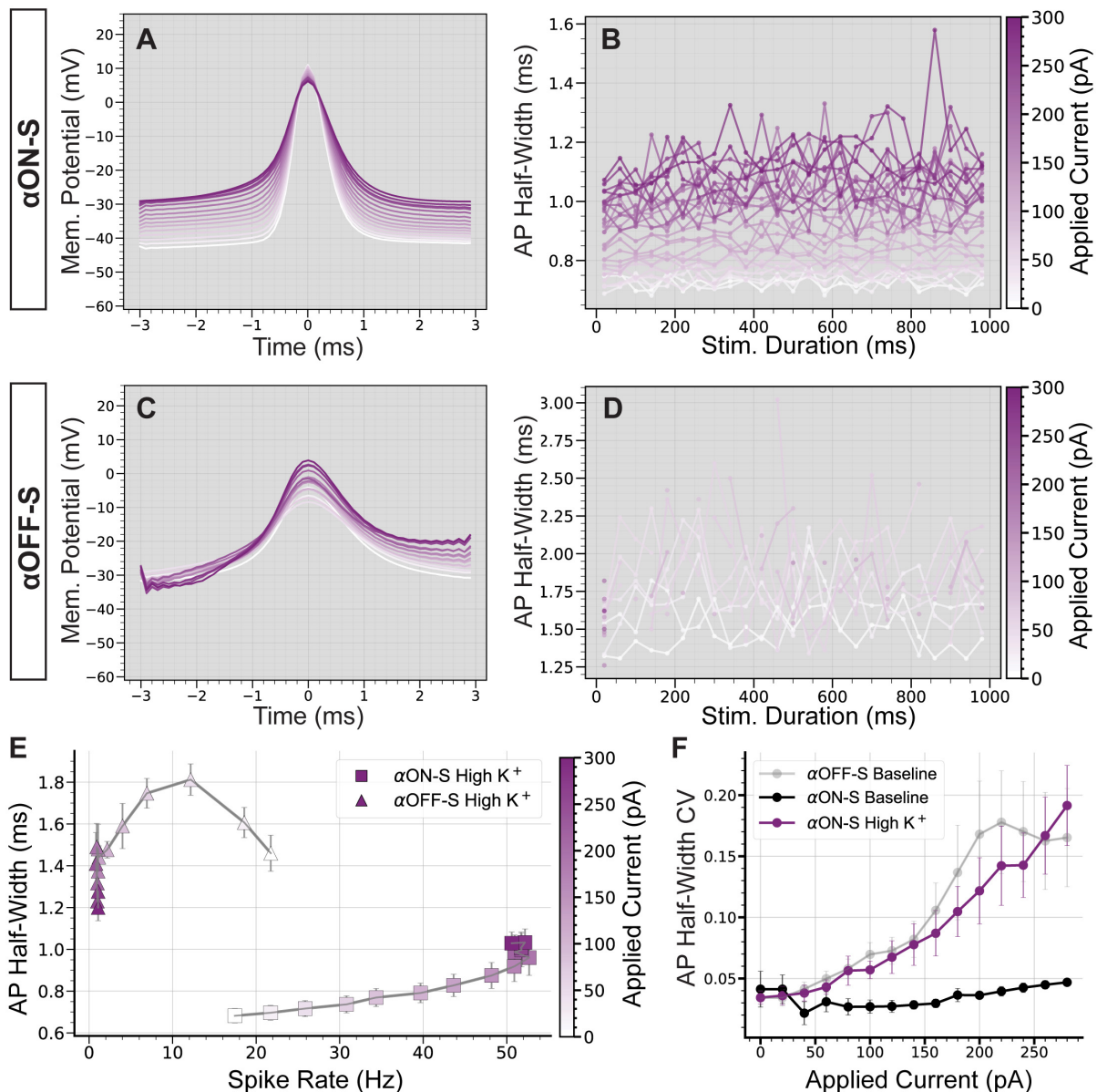


FIGURE 6

Elevated extracellular potassium significantly alters action potential shape. (A) Mean action potential (AP) shapes for alpha ON-Sustained (α ON-S) cells in high K^+ conditions at each current step. (B) Mean AP half-width vs. stimulus duration for each current level of high K^+ α ON-S cells. (C) Mean AP shapes for high K^+ alpha OFF-sustained (α OFF-S) cells at each current step. (D) Mean AP half-width vs. stimulus duration for each current level of high K^+ α OFF-S cells. (E) The mean spike rate at each current injection vs. the AP half-widths for cells in high K^+ conditions. High K^+ α ON-S retinal ganglion cells (RGCs) demonstrate significant rate-dependent spike widening (simple linear regression, non-zero slope $p < 0.0001$). (F) The coefficient of variation (CV) of AP half-widths vs. magnitude of current pulse for α ON-S before and after elevated K^+ , and comparison to α OFF-S baseline relationship. Mixed effects analysis of potassium and current on half-width for α ON-S cells shows a significant interaction between current and potassium ($p = 0.0253$). Mixed effects analysis of half-width CVs for α ON-S + high K^+ and α OFF-S at baseline demonstrates no significant difference between the groups ($p = 0.7190$). Error bars: \pm standard error of the mean.

depolarizing current increased, whereas α ON-S RGC AP half-width modestly increased in response to increasing depolarizing currents (Figures 3A–D). This AP widening phenotype closely resembles previously reported results in RGCs (Goethals et al., 2021). Stronger depolarizing currents also increased AP half-width variability in α OFF-S RGCs while α ON-S RGC

half-width variability remained constant across test currents (Figure 3E). α OFF-S RGC AP width variability increased prior to the onset of depolarization block (60–160 pA, Figure 2B), suggesting for an interaction between mechanisms generating depolarization block and maintaining AP half-width. We tested this notion by comparing AP half-width to spike

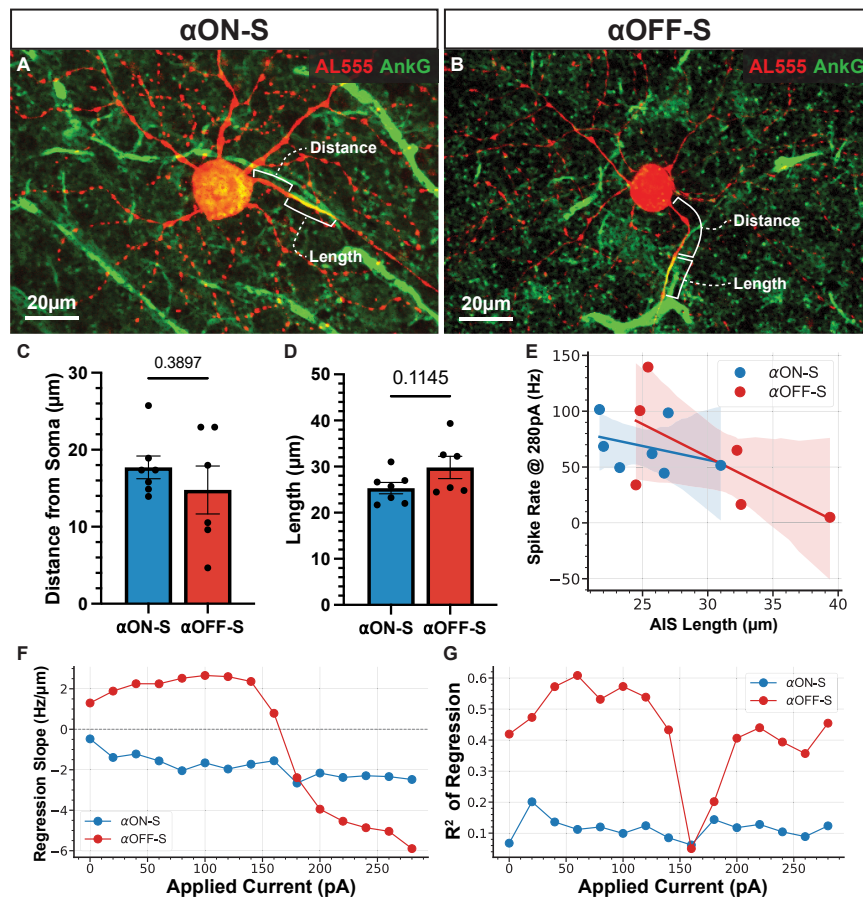


FIGURE 7
The relationship between axon initial segment (AIS) length and evoked spike rate varies by cell type and strength of stimulation. (A,B) Representative images of Alexa 555 (AL555, red) dye-filled alpha ON-Sustained (α ON-S) (A) and alpha OFF-Sustained (α OFF-S) (B) retinal ganglion cells (RGCs) labeled for the AIS protein ankyrin-G (AnkG, green). Annotations demonstrate the dimensions of AIS distance from soma and length which are quantified below. (C,D) AIS distance from soma (C) and length (D) do not differ significantly between the two RGC types ($p = 0.38397$, unpaired t -test; $p = 0.1145$, unpaired t -test). Error bars: \pm standard error of the mean. (E) Example scatter plot and linear regression best fit lines of the relationship between AIS length and current-evoked spiking rate, for 280 pA current injection. Shaded regions are 95% confidence intervals for best fit lines. (F) The slope of the regression best fit lines at each test current for α ON-S and α OFF-S RGCs. (G) R^2 values of the linear fits at each test current for α ON-S and α OFF-S RGCs.

rate for each test current (Figure 3F). We found α OFF-S RGC AP half-width significantly correlated with spike rate, but the same did not hold true for α ON-S RGCs. Our findings suggest that mechanisms generating depolarization block and regulating AP half-width are related, representing a fundamental physiologic difference between α ON-S and α OFF-S RGCs.

An overall limitation to this study is measurements of current-evoked responses under physiologic conditions may not completely isolate cell-intrinsic activity. Indeed, current injected at the soma will spread to both axonal and dendritic compartments. Depolarizing dendritic membranes will not only produce postsynaptic plasticity that influences voltage-gated activity, but also may induce presynaptic plasticity that can impact voltage-gated activity of the postsynaptic cell (Markram et al., 1997; Feldman, 2012). Notwithstanding, other

methods for measuring intrinsic responses such as genetic models, culture systems, or pharmacology may also affect intrinsic responses.

Sensitivity to extracellular K^+ underlies differences in retinal ganglion cell spiking and action potential width

Rate-dependent spike widening is driven by K^+ currents (Ma and Koester, 1996; Kasten et al., 2007). Moreover, computational modeling also links differences in K^+ permeability to the distinct stimulation thresholds for AP failure and depolarization block in ON vs. OFF RGCs (Kameneva et al., 2016). Based on this premise, we sought to probe sensitivity to K^+ gradients as a potential physiologic underpinning for

the distinct excitability profiles and AP widths we observed in α ON-S and α OFF-S cells.

Application of high K^+ medium expectedly depolarized RMP of both α RGC types but had a significantly more pronounced effect on α OFF-S RGCs (Figures 4B,C). Similarly, the current-spiking relationship for both cell types was altered (Figure 5). α ON-S cells maintained spiking activity, but additional depolarizing current input to α OFF-S cells overwhelmed spike generation capacity (Figure 5). These experiments support our key finding that α ON-S and α OFF-S RGCs have different sensitivities to the K^+ concentration gradient across their membranes. Intriguingly, the current-spiking relationship and AP shapes of α ON-S cells under high K^+ conditions closely resembled those of α OFF-S cells under baseline conditions (Figure 6). Under these conditions, α ON-S cell AP failure increased and firing rate decreased with stronger depolarizing stimulation. Furthermore, the high K^+ -induced changes in α ON-S AP shape at large depolarizations mirrored those seen in α OFF-S cells.

Evidence suggest AIS scaling mediates intrinsic excitability (Raghuram et al., 2019; Werginz et al., 2020; Wienbar and Schwartz, 2022). Thus, we investigated the scaling of the AIS as a potential contributor to differences in spike rate and depolarization block (Figure 7). For our sample, we did not detect significant differences in α ON- and α OFF-S RGC AIS dimensions (Figures 7C,D). A limitation of this study is that we did not recover the topographic location of cells in our sample, which is important because AIS dimensions can vary with retinal topography (Raghuram et al., 2019), though we have previously reported our RGC samples are biased to the mid-to-peripheral retina (Risner et al., 2018) but without bias in respect to topography (Boal et al., 2020). Intriguingly, we found that the relationship between AIS length and spike rate varied not only by cell type, but also by the strength of stimulation (Figure 7F). At low currents, α OFF-S cells with longer AISs had higher evoked spike rates. This corroborates previous evidence that AIS length is a driver of AP generation threshold (Jamann et al., 2021). However, with stronger stimulation this relationship flipped. Beyond the point where depolarization block began to occur in the majority of α OFF-S RGCs, the cells with longer AISs had lower spike rates. Furthermore, AIS length accounted but for a small amount of the variance in α ON-S cell spike rates (Figure 7G). These results support the notion that the contributions of the AIS to spiking output vary by cell type but also suggest that AIS structure cannot completely explain RGC excitability and threshold for depolarization block.

The ability of increased extracellular K^+ to shift the response properties of α ON-S toward those of α OFF-S suggests that sensitivity to extracellular K^+ is an important component shaping the different responses of the two RGC types. There are numerous potential targets for identifying the mechanistic

underpinning of this difference in K^+ sensitivity, due to the diversity of K^+ channels expressed in RGCs (Zhong et al., 2013). Channels associated with rate-dependent spike widening (as seen in Figures 3F, 6E) and modulating neuronal excitability, such as those mediating A-type voltage-gated K^+ currents (Ma and Koester, 1996; Holmqvist et al., 2002), or the Ca^{2+} -activated BK channels (Wang et al., 1998; Gu et al., 2007) may be promising for future investigation. RGC type-specific expression data (Tran et al., 2019; Goetz et al., 2022) present an opportunity to gain a detailed understanding of which channels may contribute to these physiological differences.

Linking intrinsic neuronal properties to cell-type-specific vulnerabilities to degeneration

In addition to contributing to voltage-gated responses of α ON-S and α OFF-S RGCs under physiologic conditions, the difference in K^+ sensitivity between these two cells may have important implications in a pathological context, which is an ongoing topic of investigation in our laboratory. Extracellular K^+ concentration is tightly regulated under physiologic conditions, rarely fluctuating more than a few millimolar and not exceeding 12 mM in local concentration (Heinemann and Lux, 1977). However, mechanisms regulating extracellular K^+ concentration can become disrupted in glaucoma (Fischer et al., 2019a,b), a neurodegenerative disease affecting RGCs and their axonal projection to the brain. Furthermore, select K^+ channels can contribute to RGC degeneration via interaction with apoptotic pathways (Diem et al., 2001; Koeberle et al., 2010). RGCs are a highly heterogeneous population, with different types defined by morphology, physiology, and molecular markers (Sanes and Masland, 2015; Baden et al., 2016; Bae et al., 2018; Tran et al., 2019). Importantly, certain cell types may be more vulnerable to glaucomatous degeneration than others, especially OFF RGCs, measured in terms of dendritic field size, arbor complexity, and excitability (Della Santina et al., 2013; El-Danaf and Huberman, 2015; Ou et al., 2016). Stressed RGCs exhibit enhanced excitability early in glaucoma, preceding frank degeneration (Risner et al., 2018, 2020; McGrady et al., 2020), and are metabolically restricted (Inman and Harun-Or-Rashid, 2017; Casson et al., 2021). Given type-specific differences in K^+ sensitivity, dysfunctional K^+ homeostasis in glaucoma could impose different degrees of stress on α ON-S and α OFF-S cells, influencing changes to excitability, AP generation, and sustained firing, contributing to type-specific vulnerability to disease.

Broadly, understanding intrinsic neuronal properties could offer insight into the progression of many neurodegenerative diseases, which are heterogeneous and affect a wide variety of central nervous system regions and cell types. Despite

their disparate etiologies and pathophysiologic processes, many of these diseases share common hallmark features of progression. Notably, many diseases including Alzheimer's Disease (Palop and Mucke, 2016), Parkinson's Disease (Subramaniam et al., 2014), and Amyotrophic Lateral Sclerosis (Vucic et al., 2008) also exhibit neuronal hyperexcitability early in their progression. This pathophysiologic change stresses neurons, affecting metabolic demand and calcium load, pushing neurons beyond their threshold for cellular damage toward death. Further, cell type-specific vulnerability is not unique to glaucoma (Saxena and Caroni, 2011; Fu et al., 2018). Intrinsic morphologic, physiologic, and biochemical properties might underpin increased sensitivity to degeneration during stress (Fu et al., 2018). Understanding which intrinsic properties underly selective vulnerability in disease offers insight into early degenerative mechanisms and potential therapeutic targets.

Data availability statement

The raw data supporting the conclusions of this article will be made available by the authors, without undue reservation.

Ethics statement

The animal study was reviewed and approved by Vanderbilt University Medical Center Institutional Animal Care and Use Committee.

Author contributions

AB, MR, and DC designed the research and wrote the manuscript. AB performed the research. AB and NM analyzed the data. All authors contributed to the article and approved the submitted version.

References

- Asari, H., and Meister, M. (2012). Divergence of visual channels in the inner retina. *Nat. Neurosci.* 15, 1581–1589. doi: 10.1038/nn.3241
- Baden, T., Berens, P., Franke, K., Roman Roson, M., Bethge, M., and Euler, T. (2016). The functional diversity of retinal ganglion cells in the mouse. *Nature* 529, 345–350. doi: 10.1038/nature16468
- Bae, J. A., Mu, S., Kim, J. S., Turner, N. L., Tartavull, I., Kemnitz, N., et al. (2018). Digital museum of retinal ganglion cells with dense anatomy and physiology. *Cell* 173, 1293–1306.e19. doi: 10.1016/j.cell.2018.04.040
- Boal, A., McGrady, N. R., Lambert, W. S., Risner, M. L., and Calkins, D. J. (2020). Influence of intraocular pressure on retinal ganglion cells separated by retinal quadrant. *Investig. Ophthalmol. Vis. Sci.* 61, 1995–1995.
- Cai, C., Ren, Q., Desai, N. J., Rizzo, J. F. III, and Fried, S. I. (2011). Response variability to high rates of electric stimulation in retinal ganglion cells. *J. Neurophysiol.* 106, 153–162. doi: 10.1152/jn.00956.2010
- Casson, R. J., Chidlow, G., Crowston, J. G., Williams, P. A., and Wood, J. P. M. (2021). Retinal energy metabolism in health and glaucoma. *Prog. Retin. Eye Res.* 81:100881. doi: 10.1016/j.preteyeres.2020.100881
- Cohen, E., and Sterling, P. (1990). Convergence and divergence of cones onto bipolar cells in the central area of cat retina. *Philos. Trans. R. Soc. Lond. B Biol. Sci.* 330, 323–328. doi: 10.1098/rstb.1990.0202
- Copenhagen, D. R., Hemila, S., and Reuter, T. (1990). Signal transmission through the dark-adapted retina of the toad (*Bufo marinus*). Gain, convergence, and signal/noise. *J. Gen. Physiol.* 95, 717–732. doi: 10.1085/jgp.95.4.717

Funding

Support provided by the Potocsnak Family Vision Research Center, a departmental unrestricted award by the Research to Prevent Blindness Inc. Stein Innovation Award to DC, and National Institutes of Health grants EY017427, EY024997, and EY008126 to DC. AB was supported in part by NIGMS of the National Institutes of Health under award number T32GM007347. MR was supported in part by BrightFocus Foundation Award G2022011S. Imaging supported through the Vanderbilt University Medical Center Cell Imaging Shared Resource core facility and NIH grants CA68485, DK20593, DK58404, and DK59637.

Acknowledgments

We would like to thank Tonia Rex and Sarah Naguib for providing animals used in this study and Brian Carlson for general laboratory assistance.

Conflict of interest

The authors declare that the research was conducted in the absence of any commercial or financial relationships that could be construed as a potential conflict of interest.

Publisher's note

All claims expressed in this article are solely those of the authors and do not necessarily represent those of their affiliated organizations, or those of the publisher, the editors and the reviewers. Any product that may be evaluated in this article, or claim that may be made by its manufacturer, is not guaranteed or endorsed by the publisher.

- de Polavieja, G. G., Harsch, A., Kleppe, I., Robinson, H. P., and Juusola, M. (2005). Stimulus history reliably shapes action potential waveforms of cortical neurons. *J. Neurosci.* 25, 5657–5665. doi: 10.1523/JNEUROSCI.0242-05.2005
- Della Santina, L., Inman, D. M., Lupien, C. B., Horner, P. J., and Wong, R. O. (2013). Differential progression of structural and functional alterations in distinct retinal ganglion cell types in a mouse model of glaucoma. *J. Neurosci.* 33, 17444–17457. doi: 10.1523/JNEUROSCI.5461-12.2013
- Diem, R., Meyer, R., Weishaupt, J. H., and Bähr, M. (2001). Reduction of potassium currents and phosphatidylinositol 3-kinase-dependent Akt phosphorylation by tumor necrosis factor- α rescues axotomized retinal ganglion cells from retrograde cell death *In Vivo*. *J. Neurosci.* 21, 2058–2066. doi: 10.1523/jneurosci.21-06-02058.2001
- El-Danaf, R. N., and Huberman, A. D. (2015). Characteristic patterns of dendritic remodeling in early-stage glaucoma: Evidence from genetically identified retinal ganglion cell types. *J. Neurosci.* 35, 2329–2343. doi: 10.1523/JNEUROSCI.1419-14.2015
- Emanuel, A. J., Kapur, K., and Do, M. T. H. (2017). Biophysical variation within the M1 type of ganglion cell photoreceptor. *Cell Rep.* 21, 1048–1062. doi: 10.1016/j.celrep.2017.09.095
- Famigletti, E. V. Jr., and Kolb, H. (1976). Structural basis for ON-and OFF-center responses in retinal ganglion cells. *Science* 194, 193–195. doi: 10.1126/science.959847
- Feldman, D. E. (2012). The spike-timing dependence of plasticity. *Neuron* 75, 556–571. doi: 10.1016/j.neuron.2012.08.001
- Fischer, R. A., Risner, M. L., Roux, A. L., Wareham, L. K., and Sappington, R. M. (2019a). Impairment of membrane repolarization accompanies axon transport deficits in glaucoma. *Front. Neurosci.* 13:1139. doi: 10.3389/fnins.2019.01139
- Fischer, R. A., Roux, A. L., Wareham, L. K., and Sappington, R. M. (2019b). Pressure-dependent modulation of inward-rectifying K(+) channels: Implications for cation homeostasis and K(+) dynamics in glaucoma. *Am. J. Physiol. Cell Physiol.* 317, C375–C389. doi: 10.1152/ajpcell.00444.2018
- Fu, H., Hardy, J., and Duff, K. E. (2018). Selective vulnerability in neurodegenerative diseases. *Nat. Neurosci.* 21, 1350–1358. doi: 10.1038/s41593-018-0221-2
- Galli-Resta, L., Novelli, E., Volpini, M., and Strettoi, E. (2000). The spatial organization of cholinergic mosaics in the adult mouse retina. *Eur. J. Neurosci.* 12, 3819–3822. doi: 10.1046/j.1460-9568.2000.00280.x
- Goethals, S., Sierksma, M. C., Nicol, X., Reaux-Le Goazigo, A., and Brette, R. (2021). Electrical match between initial segment and somatodendritic compartment for action potential backpropagation in retinal ganglion cells. *J. Neurophysiol.* 126, 28–46. doi: 10.1152/jn.00005.2021
- Goetz, J., Jessen, Z. F., Jacobi, A., Mani, A., Cooler, S., Greer, D., et al. (2022). Unified classification of mouse retinal ganglion cells using function, morphology, and gene expression. *bioRxiv* [Preprint]. doi: 10.1101/2021.06.10.447922
- Gu, N., Vervaeke, K., and Storm, J. F. (2007). BK potassium channels facilitate high-frequency firing and cause early spike frequency adaptation in rat CA1 hippocampal pyramidal cells. *J. Physiol.* 580(Pt 3), 859–882. doi: 10.1113/jphysiol.2006.126367
- Harden, S. W. (2022). *pyABF 2.3.5* [Online]. Available online at: <https://swharden.com/pyabf/> (accessed April 4, 22 2022).
- Heinemann, U., and Lux, H. D. (1977). Ceiling of stimulus induced rises in extracellular potassium concentration in the cerebral cortex of cat. *Brain Res.* 120, 231–249. doi: 10.1016/0006-8993(77)90903-9
- Holmqvist, M. H., Cao, J., Hernandez-Pineda, R., Jacobson, M. D., Carroll, K. I., Sung, M. A., et al. (2002). Elimination of fast inactivation in Kv4 A-type potassium channels by an auxiliary subunit domain. *Proc. Natl. Acad. Sci. U.S.A.* 99, 1035–1040. doi: 10.1073/pnas.022509299
- Inman, D. M., and Harun-Or-Rashid, M. (2017). Metabolic vulnerability in the neurodegenerative disease glaucoma. *Front. Neurosci.* 11:146. doi: 10.3389/fnins.2017.00146
- Jamann, N., Dannehl, D., Lehmann, N., Wagener, R., Thielemann, C., Schultz, C., et al. (2021). Sensory input drives rapid homeostatic scaling of the axon initial segment in mouse barrel cortex. *Nat. Commun.* 12:23. doi: 10.1038/s41467-020-20232-x
- Kameneva, T., Maturana, M. I., Hadjinicolaou, A. E., Cloherty, S. L., Ibbotson, M. R., Grayden, D. B., et al. (2016). Retinal ganglion cells: Mechanisms underlying depolarization block and differential responses to high frequency electrical stimulation of ON and OFF cells. *J. Neural Eng.* 13:016017. doi: 10.1088/1741-2560/13/1/016017
- Kasten, M. R., Rudy, B., and Anderson, M. P. (2007). Differential regulation of action potential firing in adult murine thalamocortical neurons by Kv3.2, Kv1, and SK potassium and N-type calcium channels. *J. Physiol.* 584(Pt 2), 565–582. doi: 10.1113/jphysiol.2007.141135
- Koerberle, P. D., Wang, Y., and Schlichter, L. C. (2010). Kv1.1 and Kv1.3 channels contribute to the degeneration of retinal ganglion cells after optic nerve transection in vivo. *Cell Death Differ.* 17, 134–144. doi: 10.1038/cdd.2009.113
- Krieger, B., Qiao, M., Rouso, D. L., Sanes, J. R., and Meister, M. (2017). Four alpha ganglion cell types in mouse retina: Function, structure, and molecular signatures. *PLoS One* 12:e0180091. doi: 10.1371/journal.pone.0180091
- Ma, M., and Koester, J. (1996). The role of K⁺ currents in frequency-dependent spike broadening in Aplysia R20 neurons: A dynamic-clamp analysis. *J. Neurosci.* 16, 4089–4101. doi: 10.1523/JNEUROSCI.16-13-04089.1996
- Margolis, D. J., and Detwiler, P. B. (2007). Different mechanisms generate maintained activity in ON and OFF retinal ganglion cells. *J. Neurosci.* 27, 5994–6005. doi: 10.1523/JNEUROSCI.0130-07.2007
- Margolis, D. J., Gartland, A. J., Euler, T., and Detwiler, P. B. (2010). Dendritic calcium signaling in ON and OFF mouse retinal ganglion cells. *J. Neurosci.* 30, 7127–7138. doi: 10.1523/JNEUROSCI.5694-09.2010
- Markram, H., Lubke, J., Frotscher, M., and Sakmann, B. (1997). Regulation of synaptic efficacy by coincidence of postsynaptic APs and EPSPs. *Science* 275, 213–215. doi: 10.1126/science.275.5297.213
- McGrady, N. R., Risner, M. L., Vest, V., and Calkins, D. J. (2020). TRPV1 tunes optic nerve axon excitability in glaucoma. *Front. Physiol.* 11:249. doi: 10.3389/fphys.2020.00249
- Mitra, P., and Miller, R. F. (2007a). Mechanism underlying rebound excitation in retinal ganglion cells. *Vis. Neurosci.* 24, 709–731. doi: 10.1017/S0952523807070654
- Mitra, P., and Miller, R. F. (2007b). Normal and rebound impulse firing in retinal ganglion cells. *Vis. Neurosci.* 24, 79–90. doi: 10.1017/S0952523807070101
- Ou, Y., Jo, R. E., Ullian, E. M., Wong, R. O., and Della Santina, L. (2016). Selective vulnerability of specific retinal ganglion cell types and synapses after transient ocular hypertension. *J. Neurosci.* 36, 9240–9252. doi: 10.1523/JNEUROSCI.0940-16.2016
- Palop, J. J., and Mucke, L. (2016). Network abnormalities and interneuron dysfunction in Alzheimer disease. *Nat. Rev. Neurosci.* 17, 777–792. doi: 10.1038/nrn.2016.141
- Pang, J. J., Gao, F., and Wu, S. M. (2003). Light-evoked excitatory and inhibitory synaptic inputs to ON and OFF alpha ganglion cells in the mouse retina. *J. Neurosci.* 23, 6063–6073. doi: 10.1523/JNEUROSCI.23-14-06063.2003
- Pillow, J. W., Paninski, L., Uzzell, V. J., Simoncelli, E. P., and Chichilnisky, E. J. (2005). Prediction and decoding of retinal ganglion cell responses with a probabilistic spiking model. *J. Neurosci.* 25, 11003–11013. doi: 10.1523/JNEUROSCI.3305-05.2005
- Raghuram, V., Werginz, P., and Fried, S. I. (2019). Scaling of the AIS and somatodendritic compartments in alpha S RGCs. *Front. Cell. Neurosci.* 13:436. doi: 10.3389/fncel.2019.00436
- Risner, M. L., McGrady, N. R., Boal, A. M., Pasini, S., and Calkins, D. J. (2020). TRPV1 supports axogenic enhanced excitability in response to neurodegenerative stress. *Front. Cell. Neurosci.* 14:603419. doi: 10.3389/fncel.2020.603419
- Risner, M. L., Pasini, S., Cooper, M. L., Lambert, W. S., and Calkins, D. J. (2018). Axogenic mechanism enhances retinal ganglion cell excitability during early progression in glaucoma. *Proc. Natl. Acad. Sci. U.S.A.* 115, E2393–E2402. doi: 10.1073/pnas.1714888115
- Risner, M. L., Pasini, S., McGrady, N. R., and Calkins, D. J. (2022). Bax contributes to retinal ganglion cell dendritic degeneration during glaucoma. *Mol. Neurobiol.* 59, 1366–1380. doi: 10.1007/s12035-021-02675-5
- Risner, M. L., Pasini, S., McGrady, N. R., D'Alessandro, K. B., Yao, V., Cooper, M. L., et al. (2021). Neuroprotection by Wld(S) depends on retinal ganglion cell type and age in glaucoma. *Mol. Neurodegener.* 16:36. doi: 10.1186/s13024-021-00459-y
- Sanes, J. R., and Masland, R. H. (2015). The types of retinal ganglion cells: Current status and implications for neuronal classification. *Annu. Rev. Neurosci.* 38, 221–246. doi: 10.1146/annurev-neuro-071714-034120
- Saxena, S., and Caroni, P. (2011). Selective neuronal vulnerability in neurodegenerative diseases: From stressor thresholds to degeneration. *Neuron* 71, 35–48. doi: 10.1016/j.neuron.2011.06.031
- Shekhar, K., and Sanes, J. R. (2021). Generating and using transcriptomically based retinal cell atlases. *Annu. Rev. Vis. Sci.* 7, 43–72. doi: 10.1146/annurev-visual-032621-075200
- Sladek, A. L., and Nawy, S. (2020). Ocular hypertension drives remodeling of AMPA receptors in select populations of retinal ganglion cells. *Front. Synaptic Neurosci.* 12:30. doi: 10.3389/fnsyn.2020.00030

- Subramaniam, M., Althof, D., Gispert, S., Schwenk, J., Auburger, G., Kulik, A., et al. (2014). Mutant alpha-synuclein enhances firing frequencies in dopamine substantia nigra neurons by oxidative impairment of A-type potassium channels. *J. Neurosci.* 34, 13586–13599. doi: 10.1523/JNEUROSCI.5069-13.2014
- Tran, N. M., Shekhar, K., Whitney, I. E., Jacobi, A., Benhar, I., Hong, G., et al. (2019). Single-cell profiles of retinal ganglion cells differing in resilience to injury reveal neuroprotective genes. *Neuron* 104, 1039–1055.e12. doi: 10.1016/j.neuron.2019.11.006
- Twyford, P., Cai, C., and Fried, S. (2014). Differential responses to high-frequency electrical stimulation in ON and OFF retinal ganglion cells. *J. Neural Eng.* 11:025001. doi: 10.1088/1741-2560/11/2/025001
- Uzzell, V. J., and Chichilnisky, E. J. (2004). Precision of spike trains in primate retinal ganglion cells. *J. Neurophysiol.* 92, 780–789. doi: 10.1152/jn.01171.2003
- Virtanen, P., Gommers, R., Oliphant, T. E., Haberland, M., Reddy, T., Cournapeau, D., et al. (2020). SciPy 1.0: Fundamental algorithms for scientific computing in Python. *Nat. Methods* 17, 261–272. doi: 10.1038/s41592-019-0686-2
- Vucic, S., Nicholson, G. A., and Kiernan, M. C. (2008). Cortical hyperexcitability may precede the onset of familial amyotrophic lateral sclerosis. *Brain* 131(Pt 6), 1540–1550. doi: 10.1093/brain/awn071
- Wang, G. Y., Robinson, D. W., and Chalupa, L. M. (1998). Calcium-activated potassium conductances in retinal ganglion cells of the ferret. *J. Neurophysiol.* 79, 151–158. doi: 10.1152/jn.1998.79.1.151
- Werginz, P., Raghuram, V., and Fried, S. I. (2020). Tailoring of the axon initial segment shapes the conversion of synaptic inputs into spiking output in OFF- α T retinal ganglion cells. *Sci. Adv.* 6:eabb6642. doi: 10.1126/sciadv.abb6642
- Wienbar, S., and Schwartz, G. W. (2022). Differences in spike generation instead of synaptic inputs determine the feature selectivity of two retinal cell types. *Neuron* 110, 2110–2123.e4. doi: 10.1016/j.neuron.2022.04.012
- Zhong, Y. S., Wang, J., Liu, W. M., and Zhu, Y. H. (2013). Potassium ion channels in retinal ganglion cells (review). *Mol. Med. Rep.* 8, 311–319. doi: 10.3892/mmr.2013.1508